Thermal conductivity in complex metallic alloys: Beyond Wiedemann-Franz law

Enrique Maciá*
Departamento de Física de Materiales, Facultad CC. Físicas, Universidad Complutense de Madrid, E-28040 Madrid, Spain
(Received 31 March 2009; revised manuscript received 5 May 2009; published 10 June 2009)

In this work we consider the range of validity of the Wiedemann-Franz law (WFL) in quasicrystals, approximant phases, and giant unit-cell complex metallic alloys. In the limit of very low temperatures the WFL is satisfied, as expected, but as the temperature is progressively increased the Lorenz function deviates from the ideal behavior $L(T)/L_0=1$. Whereas the quasicrystalline sample exhibits a systematic and significant deviation for all considered temperatures, the other samples show the existence of a characteristic temperature signaling the onset of the anomalous behavior. This characteristic temperature is directly related to the unit-cell density of the sample and progressively takes on larger values as this density decreases. An alternative route to derive the lattice contribution to the thermal conductivity based on a simultaneous fitting analysis of the electrical conductivity $\sigma(T)$ and thermoelectric-power $S(T)$ experimental transport curves is proposed. The capabilities of this approach are illustrated by studying the temperature dependence of the lattice contribution to the thermal conductivity in the ξ'-AlPdMn giant unit-cell phase.

DOI: 10.1103/PhysRevB.79.245112 PACS number(s): 61.44.Br, 71.23.Ft, 72.15.Cz

I. INTRODUCTION

Complex metallic alloys (CMAs) are either periodic or aperiodic crystalline compounds of the family of intermetallics that are characterized by giant unit cells (containing up to thousands of atoms) and the occurrence of structural clusters, where icosahedrally coordinated environments play a prominent role.[1] The structure of CMAs thus shows duality; on the scale of several nanometers, these alloys exhibit a well-defined atomic long-range order, whereas on a shorter scale, they locally resemble cluster aggregates. The presence of two physically relevant length scales—one defined by the unit-cell parameters and the other by the cluster substructure—may have a significant impact on the physical properties of these materials, such as the electronic structure and lattice dynamics. On this basis, CMAs are expected to exhibit remarkable transport properties, such as a combination of metallic electrical conductivity with low thermal conductivity, or tunable electrical and thermal resistances by varying the composition.[2]

The thermal conductivity of CMAs belonging to different families has been measured during the last decade, covering both low- and high-temperature ranges. From the collected data some general conclusions can be drawn: (1) the thermal conductivity of CMAs is unusually low as compared to that of typical metallic alloys, (2) the contribution of electrons to the thermal transport is significantly lower than that due to phonons over a wide temperature range in CMAs, and (3) their thermal diffusivity is extraordinarily low.[3,4] In order to get a suitable physical picture of the basic mechanisms determining thermal conduction in CMAs, some fundamental problems should be properly addressed. Among these fundamental issues we have the probable presence of different physical processes at work at different temperature regimes, the existence of interactions coupling the dynamics of electrons and phonons, and the existence of two relevant spatial scales in cluster-based solids. Albeit the full-fledged problem is quite complex, the low thermal conductivity of these materials, especially in the case of quasicrystals and related approximant phases, can be understood in terms of two main facts. First, the charge-carrier concentration is significantly low so that heat must mainly propagate by means of atomic vibrations (phonons). Second, in the energy window where lattice thermal transport is expected to be most efficient the frequency spectrum is highly fragmented. As a consequence, the corresponding eigenstates exhibit very small group velocities and thermal transport is further reduced.[5] In particular, quasicrystal lattices have a fractal reciprocal space, lacking a well-defined lower bond as that provided by the lattice parameter in the case of periodic crystals. Consequently, the transfer of momentum to the lattice is not bounded below, giving rise to a significant degradation of thermal current through the sample.

Generally, in order to estimate the lattice contribution to the thermal conductivity $\kappa_l(T)$, the Wiedemann-Franz law (WFL) has been routinely applied in the study of the thermal transport properties of CMAs. As it is well known, this law links the electrical conductivity, $\sigma(T)$, and the charge carriers' contribution to the thermal conductivity, $\kappa_e(T)$, of a substance by means of the relationship $\kappa_e(T)=L_0T\sigma(T)$, where T is the temperature and $L_0=(k_B/e)^2\eta_0$ is the Lorenz number, where k_B is the Boltzmann constant, e is the electron charge, and η_0 depends on the sample's nature (for metallic systems $\eta_0=\pi^2/3$, and we get Sommerfeld's value $L_0=2.44\times10^{-8}$ V K^{-2}, while for semiconductors $\eta_0\simeq2$). The standard procedure to estimate the lattice contribution to the thermal conductivity entirely relies on the validity of the WFL by subtracting to the experimental data, $\kappa_m(T)$, the expected electronic contribution to obtain

$$\kappa_l(T)=\kappa_m(T)-L_0T\sigma. \quad (1)$$

In this way, the ratio κ_e/κ_l has been determined for several CMA representatives at room temperature (Table I). Keeping in mind that this ratio takes on values within the range of 10–100 for conventional alloys, one realizes that the thermal transport of CMAs is largely dominated by phonons at room temperature.

TABLE I. Values of the ratio κ_e/κ_l at $T=300$ K for different CMAs derived from the $\kappa_m(T)$ and $\sigma(T)$ experimental transport curves reported in the literature making use of Eq. (1).

κ_e/κ_l	Quasicrystals	Approximants	Clathrates
5–1	*i*-ZnMgY[a]	Bergman[b]	$Y_3Ir_4Ge_{14}$ [c]
~1	*i*-AgInYb[d]	Cd_6Yb [e]	$Eu_8Ga_{16}Ge_{30}$ [f]
0.5–0.01	*i*-AlPd(Mn,Re)[g]	1/1-AlReSi[h]	

[a]Reference 6.
[b]Reference 7.
[c]Reference 8.
[d]Reference 9.
[e]Reference 10.
[f]Reference 11.
[g]References 12 and 13.
[h]Reference 14.

Physically, the WFL expresses a transport symmetry arising from the fact that the motion of the carriers determines both the electrical and thermal currents at low temperatures. As the temperature of the sample is progressively increased, the validity of WFL will depend on the nature of the interaction between the charge carriers and the different scattering sources present in the solid. In general, the WFL applies as far as elastic processes dominate the transport coefficients and usually holds for arbitrary band structures provided that the change in energy due to collisions is small compared with k_BT.[15] Accordingly, one expects some appreciable deviation from WFL when electron-phonon interactions, affecting the electrical and heat currents in a dissimilar way, start to play a significant role.[16] On the other hand, at high enough temperatures the heat transfer is dominated by the charge carriers again, due to umklapp phonon-scattering processes, and the WFL is expected to hold as well. Nonetheless, since transport properties of most CMAs are quite unusual by the standard of common metallic alloys, it seems convenient to check up on the validity of this law for these materials since our understanding of their thermal properties should be substantially revised if it does not hold.[17–20]

A suitable experimental measure of the WFL validity over a given temperature range can be obtained from the study of the magnitude $\kappa_m(T)/\sigma(T)=TL(T)+\varphi(T)$, where the so-called Lorenz function is defined by the relationship

$$L(T) \equiv \frac{\kappa_e(T)}{T\sigma(T)} \tag{2}$$

and $\varphi(T)$ accounts for the phonon contribution to the heat transport. A study of the temperature variation in the κ_m/σ ratio in several intermetallic compounds showed that the experimental data may be fitted by a linear temperature dependence of the form $\kappa_m/\sigma=LT+B$ over the temperature range of 350–800 K.[3,21] By comparing the slopes obtained for pure aluminum and icosahedral AlCuFe samples the ratio $L_{QC}/L_{Al}\simeq 1.21$ was obtained, hence indicating an enhanced Lorenz number for quasicrystalline alloys at high temperatures. In a similar way, room-temperature $L(T)$ values larger than L_0 were experimentally reported for other CMAs, hence suggesting the convenience of introducing a slightly modified expression of the form

TABLE II. Values of the enhancement parameter ε for different CMAs reported in the literature. The ε values were obtained from a fitting analysis of the thermal-conductivity experimental curves making use of Eq. (3).

ε	Sample	Ref.
−0.002	γ-AlCrFe	22
0.03	Ψ-AlPdMn	23
0.14	O_1/O_2-AlCrFe	22
0.16	ξ'-AlPdMn	23
0.43	*i*-$Zn_{57}Mg_{34}Y_9$	6
1.1	*i*-$Al_{64}Cu_{23}Fe_{13}$	24

$$\kappa_e(T) = (1+\varepsilon)L_0T\sigma(T) \tag{3}$$

in order to accurately describe experimental data (Table II). By inspecting this table we see that the enhancement parameter ε is related to the structural complexity of the underlying lattice taking on progressively larger values as a fully three-dimensional quasiperiodic order is approached in the considered sample. Accordingly, there exists experimental evidence indicating that Eq. (1) does not provide an accurate enough expression to properly derive the lattice contribution $\kappa_l(T)$ from the measured thermal conductivity in this materials' class.

This shortcoming significantly hampers a proper understanding of heat transfer mechanisms in CMAs, especially for quasicrystals and their related approximants. In fact, during the last decade some specific treatments, aimed to exploit the physical implications of the quasiperiodic order notion, have been introduced in the theory of thermal transport in these materials. Thus, the lack of a well-defined reciprocal lattice in quasicrystals leads to a power-law (instead of the usual exponential) dependence of the umklapp processes which can be expressed in terms of a scattering rate of the form $\tau^{-1}\propto\omega^2T^4$, where ω is the phonon frequency.[25] These processes are expected to be dominant in the temperature range $20\lesssim T\lesssim 100$. Making use of this scattering rate value in the expression

$$\kappa_l(T) \sim T^3\int_0^{\Theta/T}\frac{x^4e^x}{(e^x-1)^2}\tau(x)dx, \tag{4}$$

where $x\equiv\frac{\hbar\omega}{k_BT}$, one gets $\kappa_l\sim T^{-3}$. According to the data listed in Table III, however, fitting analyses to experimentally derived κ_l curves do not agree with theoretical expectations since the obtained scattering rates differ from the expected one, leading to a temperature dependence of the form $\kappa_l\sim T^{-1}$ in all considered cases. On the other hand, starting at $T\gtrsim 100$ K one expects the variable-range hopping mechanism introduced by Janot[28] will play an increasingly significant role. According to this model the thermal-conductivity curve should rise following a power law of the form $\kappa_l\sim T^{3/2}$ within the temperature interval $100\lesssim T\lesssim 400$. Nevertheless, the fitting analysis to experimentally derived κ_l curves shown in Table IV indicates that most considered samples deviate from the expected behavior in this tempera-

TABLE III. Values of the umklapp scattering rate τ and the lattice thermal-conductivity temperature dependence $\kappa_l(T)$ for different CMAs reported in the literature. The τ functional dependences were obtained from a fitting analysis of the thermal-conductivity experimental curves and the κ_l temperature dependence was derived from Eq. (4).

Sample	τ^{-1}	$\kappa_l(T)$	Ref.
i-$Zn_{57}Mg_{34}Y_9$	$\omega^3 T$	T^{-1}	6
i-$Al_{64}Cu_{23}Fe_{13}$	$\omega^3 T$	T^{-1}	24
i-$Al_{72}Pd_{19.5}Mn_{18.5}$	$\omega^2 T$	T^{-1}	26
γ-AlCrFe	$\omega^2 T$	T^{-1}	22
ε-AlPd(Fe,Co,Rh)	$\omega^2 T$	T^{-1}	27
Ψ-AlPdMn	ω^4	T^{-1}	23
ξ'-AlPdMn	ω^4	T^{-1}	23

ture range. In the light of these results, the question naturally arises concerning as to whether such a disagreement is due to a fundamental reason (that is, the proposed theoretical mechanisms are inappropriate) or rather it merely expresses a flawed derivation of the considered $\kappa_l(T)$ curves as obtained from Eq. (1).

Spurred by these physical motivations in this work we will address a detailed study of the charge-carrier contribution to the thermal conductivity in order to check for the applicability of the standard approach based on the systematic application of the WFL as given by Eq. (1) or (3). From this study, we will propose the use of an alternative route, based on a combined analysis of *both* the $\sigma(T)$ and $S(T)$ transport coefficients, in order to properly reduce experimental data regarding $\kappa_l(T)$ in a systematic way. To this end, we will derive analytical expressions for $\kappa_e(T)$ and $L(T)$ and we will use them to extract suitable information regarding the lattice contribution to the thermal conductivity. The required analytical expressions are fully derived in Sec. II and the obtained results are discussed in Sec. III within the framework of a phenomenological approach which allows for a direct comparison with suitable experimental data. Finally, the main conclusions of this work are presented in Sec. IV along with some suggestions for additional research.

TABLE IV. Reported values of the power-law exponent describing the lattice thermal-conductivity temperature dependence $\kappa_l(T) \sim T^n$ for different quasicrystals. The n values were obtained from a fitting analysis of the thermal-conductivity curves in the indicated temperature ranges.

Sample	T range (K)	n	Ref.
i-CdYb	110–300	1.2	10
i-AlPdRe	150–300	1.4	9
i-AgInYb	150–300	1.5	13
i-AlPdMn	200–300	1.7	12
i-ZnMgY	140–300	1.7	6

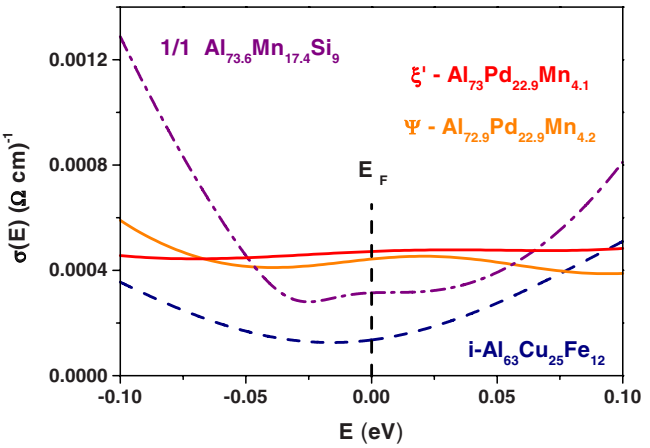

FIG. 1. (Color online) The spectral-conductivity curves for ξ'-AlPdMn and Ψ-AlPdMn giant unit-cell samples are compared to those corresponding to the $Al_{63}Cu_{25}Fe_{12}$ icosahedral quasicrystal (dashed) and the $Al_{73.6}Mn_{17.4}Si_9$ 1/1 cubic approximant phase (dot dashed).

II. ANALYTICAL RESULTS

Following previous works we shall start by considering a realistic model for the electronic structure of certain CMAs in terms of the spectral-conductivity function given by[29]

$$\sigma(E) = \bar{\sigma}\left\{\frac{\gamma_1}{(E-\delta_1)^2+\gamma_1^2} + \frac{\alpha\gamma_2}{(E-\delta_2)^2+\gamma_2^2}\right\}^{-1}, \qquad (5)$$

which satisfactorily describes the electronic structure of several CMAs in terms of a wide Lorentzian peak (related to the Fermi-surface Brillouin-zone interaction) plus a narrow Lorentzian peak (related to *sp-d* hybridization effects).[30,31] This model includes six parameters, determining Lorentzian's heights ($\bar{\sigma}/\gamma_i$) and widths ($\sim\gamma_i$), their positions with respect to the Fermi level, δ_i, and their relative weight in the overall structure, $\alpha > 0$. The parameter $\bar{\sigma}$ is a scale factor measured in $(\Omega\ \mathrm{cm\ eV})^{-1}$ units. Suitable values for these electronic model parameters can be obtained by properly combining *ab initio* calculations of approximant phases with experimental transport data of CMAs within a phenomenological approach.[32–34] For the sake of illustration, in Fig. 1 we show the resulting spectral-conductivity functions for several representative samples whose model parameters are listed in Table V. We see that the spectral-conductivity curves of both quasicrystalline and approximant phases are deeper at Fermi energy and steeper in the wings, indicating the existence of a well-defined pseudogap in both compounds. The $\sigma(E)$ curves of the ξ' and Ψ-AlPdMn samples are relatively flat as compared to those corresponding to $Al_{63}Cu_{25}Fe_{12}$ and $Al_{73.6}Mn_{17.4}Si_9$ compounds. The absence of such a well-defined pseudogap in the case of ξ' and Ψ-AlPdMn samples indicates that the electrical conductivity is consequently higher. Thus, the origin of the almost temperature-independent electrical conductivity reported for both the ξ' and Ψ-AlPdMn alloys[24] can be then traced back to the specific form of the spectral conductivity, which exhibits very weak variation over the energy scale of several meV around the Fermi level. Yet, they show some fine struc-

TABLE V. Electronic model parameters for four representative CMAs.

Sample	α	δ_1 (meV)	δ_2 (meV)	γ_1 (meV)	γ_2 (meV)	Ref.
i-$Al_{63}Cu_{25}Fe_{12}$	1.07	−5	−16	587	55	35
$1/1Al_{73.6}Mn_{17.4}Si_9$	0.21	23	−29	65	22	33
ξ'-$Al_{73}Pd_{22.9}Mn_{4.1}$	1.42	109	−92	130	145	34
Ψ-$Al_{72.9}Pd_{22.9}Mn_{4.2}$	0.83	102	−50	86	81	This work

ture that yields observable effects in the temperature-dependent thermoelectric power curves.[24] These electronic structure related effects highlight the difference between ξ' and Ψ-AlPdMn phases and conventional free-electron alloys.

The temperature-dependent transport coefficients can be obtained from the knowledge of the spectral-conductivity function by means of the Kubo-Greenwood version of the linear-response theory. Within this approach the electrical, **j**, and thermal, **h**, current densities are, respectively, related to the voltage and temperature gradients according to the expression

$$\begin{pmatrix} \mathbf{j} \\ \mathbf{h} \end{pmatrix} = \begin{pmatrix} \mathcal{L}_{11} & \mathcal{L}_{12} \\ \mathcal{L}_{21} & \mathcal{L}_{22} \end{pmatrix} \begin{pmatrix} -\nabla V \\ -\nabla T \end{pmatrix}. \tag{6}$$

The central information quantities are the kinetic coefficients

$$\mathcal{L}_{ij}(T) = (-1)^{i+j} \int \sigma(E)(E-\mu)^{i+j-2} \left(-\frac{\partial f}{\partial E}\right) dE, \tag{7}$$

where $f(E,\mu,T)$ is the Fermi-Dirac distribution function, E is the electron energy, and μ is the chemical potential. In this formulation all the microscopic details of the system are included in the $\sigma(E)$ function. From the knowledge of the kinetic coefficients one obtains the electrical conductivity

$$\sigma(T) = \mathcal{L}_{11}(T), \tag{8}$$

the thermoelectric power,

$$S(T) = \frac{1}{|e|T} \frac{\mathcal{L}_{12}(T)}{\sigma(T)}, \tag{9}$$

the electronic thermal conductivity,

$$\kappa_e(T) = \frac{1}{e^2 T} \mathcal{L}_{22}(T) - T\sigma(T)S(T)^2, \tag{10}$$

and the Lorenz function in a unified way. As a first approximation one generally assumes $\mu(T) \approx E_F$.[36] Then, by expressing Eqs. (8)–(10) in terms of the scaled variable $x \equiv (E-\mu)\beta$, where $\beta \equiv (k_B T)^{-1}$, the transport coefficients can be rewritten as

$$\sigma(T) = \frac{J_0}{4}, \tag{11}$$

$$S(T) = -\frac{k_B}{|e|} \frac{J_1}{J_0}, \tag{12}$$

$$\kappa_e(T) = \frac{k_B^2 T}{4e^2 J_0} \begin{vmatrix} J_0 & J_1 \\ J_1 & J_2 \end{vmatrix}, \tag{13}$$

$$L(T) = \left(\frac{k_B}{eJ_0}\right)^2 \begin{vmatrix} J_0 & J_1 \\ J_1 & J_2 \end{vmatrix} \tag{14}$$

in terms of the reduced kinetic coefficients

$$J_n = \int_{-\infty}^{\infty} x^n \sigma(x) \mathrm{sech}^2(x/2) dx. \tag{15}$$

Making use of Eq. (5) these kinetic coefficients can be expressed in the form[32]

$$\begin{aligned} J_0 c_0^{-1} &= B\beta^{-2} + a_0 G_0(\beta) + n_0 H_0(\beta) + a_3 \beta^{-1} H_1(\beta), \\ J_1 c_0^{-1} &= B a_1 \beta^{-1} + a_3 \beta G_0(\beta) + a_5 H_1(\beta), \\ J_2 c_0^{-1} &= B a_0 + \frac{21}{20} B^2 \beta^{-2} + a_5 \beta^2 G_0(\beta) + a_6 \beta H_1(\beta), \end{aligned} \tag{16}$$

where $c_0 \equiv \bar{\sigma}(\gamma_1 + \alpha\gamma_2)^{-1}$, $B \equiv 4\pi^2/3$, and the coefficients a_i are given by

$$\begin{aligned} a_1 &= 2(q_1 - n_3), \\ a_0 &= 4q_1^2 - 4q_1 n_3 + n_2 - q_0, \\ a_3 &= 8q_1^3 - 8q_1^2 n_3 + 2q_1 n_2 - 4q_1 q_0 + 2q_0 n_3 - 2n_1, \\ a_4 &= n_0 - 4q_0 q_1^2 + 4q_0 q_1 n_3 - q_0 n_2 + q_0^2, \\ a_5 &= 2a_3 q_1 + a_4, \quad a_6 = 2a_5 q_1 - a_3 q_0, \end{aligned} \tag{17}$$

with $n_0 \equiv \varepsilon_1^2 \varepsilon_2^2$, $\varepsilon_i^2 \equiv \gamma_i^2 + \delta_i^2$, $n_1 = \delta_1 \varepsilon_2^2 + \delta_2 \varepsilon_1^2$, $n_2 = \varepsilon_1^2 + \varepsilon_2^2 + 4\delta_1\delta_2$, $n_3 = \delta_1 + \delta_2$, $q_0 \equiv n_0(\gamma_1 \varepsilon_1^{-2} + \alpha\gamma_2 \varepsilon_2^{-2})(\gamma_1 + \alpha\gamma_2)^{-1}$, and $q_1 = (\gamma_1\delta_2 + \alpha\delta_1\gamma_2)(\gamma_1 + \alpha\gamma_2)^{-1}$. We have also introduced the auxiliary functions $G_0(\beta) \equiv 4 - q_0 H_0(\beta)$ and

$$H_k(\beta) \equiv \beta^2 \int_{-\infty}^{\infty} \frac{x^k \, \mathrm{sech}^2(x/2)}{(x - pA\beta)^2 + (A\beta)^2} dx, \tag{18}$$

where $A \equiv \sqrt{q_0 - q_1^2}$ and $p \equiv q_1/A$. Explicit evaluation gives

$$A = \frac{\sqrt{(1+\alpha)^2 \gamma_1^2 \gamma_2^2 + \alpha\gamma_1\gamma_2[(\gamma_1 - \gamma_2)^2 + (\delta_1 - \delta_2)^2]}}{\gamma_1 + \alpha\gamma_2}$$

so that $A > 0$ for any possible spectral-conductivity model. Taking into account the Fourier-transform relationships,[37]

$$\frac{1}{u^2+c^2}=\frac{1}{2c}\int_{-\infty}^{\infty}e^{-c|\omega|}e^{i\omega u}d\omega, \tag{19}$$

$$\frac{u}{u^2+c^2}=-\frac{i}{2}\int_{-\infty}^{\infty}e^{-c|\omega|}e^{i\omega u}\,\mathrm{sgn}(\omega)d\omega, \tag{20}$$

the functions H_0 and H_1 can be properly rearranged in the following forms:

$$H_0(\beta)=\frac{\beta}{2A}\int_{-\infty}^{\infty}e^{-c|\omega|}e^{-ipc\omega}d\omega\int_{-\infty}^{\infty}e^{i\omega x}\,\mathrm{sech}^2(x/2)dx,$$

$$H_1(\beta)=q_1\beta H_0-\frac{i\beta^2}{2}\int_{-\infty}^{\infty}e^{-c\omega(\mathrm{sgn}(\omega)+ip)}\,\mathrm{sgn}(\omega)d\omega$$

$$\times\int_{-\infty}^{\infty}e^{i\omega x}\,\mathrm{sech}^2(x/2)dx, \tag{21}$$

where $c\equiv A\beta>0$. Making use of the Fourier transform

$$\int_{-\infty}^{\infty}e^{i\omega x}\,\mathrm{sech}^2(x/2)dx=4\pi\omega\,\mathrm{csch}(\pi\omega) \tag{22}$$

one finally obtains[38]

$$H_0(\beta)=\frac{\beta}{\pi A}[\psi_1(z)+\psi_1(z^*)],$$

$$H_1(\beta)=\frac{i\beta^2}{\pi}[s^*\psi_1(z^*)-s\psi_1(z)] \tag{23}$$

in terms of the trigamma function,[39]

$$\psi_1(z)=\frac{d^2}{dz^2}\ln\Gamma(z), \tag{24}$$

where $\Gamma(z)$ is Euler's gamma function, $s\equiv 1+ip$, and $z\equiv 1/2+s\bar{\beta}/2$, with $\bar{\beta}\equiv A\beta/\pi$. The H_k functions contain physical information regarding the temperature dependence of the transport coefficients. At high enough temperatures $(\beta\to 0)$ we have $z=z^*\to 1/2$, so that $\psi_1(z)=\psi_1(z^*)\to\psi_1(1/2)=\pi^2/2$. In that case, plugging Eq. (23) into Eq. (16) one obtains the following asymptotic expressions for the kinetic coefficients

$$J_0\to Bc_0\beta^{-2},\quad J_1\to Bc_0a_1\beta^{-1},\quad J_2\to\frac{21}{20}B^2c_0\beta^{-2}$$

and substituting them into Eqs. (11)–(14) the following high-temperature expressions are obtained for the transport coefficients

$$\sigma(T)\simeq c_0bT^2,\quad S(T)\simeq-\frac{a_1}{|e|T},\quad k_e(T)\simeq\frac{21}{5}c_0L_0bT^3,$$

where $b\equiv e^2L_0=2.44\times10^{-8}$ $(\mathrm{eV})^2\,\mathrm{K}^{-2}$. As we can see, the electrical and thermal conductivities exhibit a parabolic and cubic growth with temperature, respectively. The Seebeck coefficient becomes vanishingly small as the temperature is increased and the Wiedemann-Franz law is satisfied in the high-temperature regime, though asymptotic Lorenz's number value $L(T)\to 21L_0/5$ is significantly larger than L_0, in general agreement with some experimental results described in Sec. I.

In order to properly analyze the remaining temperature range it is convenient to rewrite Eq. (23) by using the relationship $\psi_1(z)=\zeta(2,z)$, where $\zeta(s,z)\equiv\Sigma_{k=0}^{\infty}(k+z)^{-s}$ is the Hurwitz zeta function, which reduces to the Riemann zeta function in the case $z=1$.[39] In this way, one readily realizes that in the ideal quasiperiodic limit $q_1\to 0$ discussed in Ref. 20 (i.e., $z=z^*=1/2+\tilde{\beta}$, with $\tilde{\beta}\equiv\sqrt{q_0}\beta/2\pi$), Eq. (23) reduces to $H_0=4q_0^{-1}\tilde{\beta}\zeta(2,1/2+\tilde{\beta})$ and $H_1=0$, as it was previously reported. The Hurwitz zeta function admits the integral representation,[40]

$$\zeta(s,z)=\frac{1}{\Gamma(s)}\int_0^{\infty}\frac{e^{-zt}}{1-e^{-t}}t^{s-1}dt, \tag{25}$$

which is valid for $\mathrm{Re}(s)>1$ and $\mathrm{Re}(z)>0$. In our case $\mathrm{Re}(2)>1$ and $\mathrm{Re}(z)=1/2+\beta A/2\pi>0$ so that both conditions are satisfied. Making use of Eq. (25) we introduce the auxiliary integrals,

$$I_+(\beta)\equiv\psi_1(z)+\psi_1(z^*)=4\bar{\beta}^{-2}\int_0^{\infty}\frac{\varphi e^{-\varphi}\cos(p\varphi)d\varphi}{\sinh(\varphi/\bar{\beta})},$$

$$I_-(\beta)\equiv i[\psi_1(z)-\psi_1(z^*)]=4\bar{\beta}^{-2}\int_0^{\infty}\frac{\varphi e^{-\varphi}\sin(p\varphi)d\varphi}{\sinh(\varphi/\bar{\beta})}, \tag{26}$$

where $\varphi\equiv\bar{\beta}t/2$. We now replace the hyperbolic function in Eq. (26) by its Taylor-series expansion

$$\mathrm{csch}(\bar{\beta}^{-1}\varphi)=\frac{A\beta}{\pi\varphi}\left(1+\sum_{n=1}^{\infty}A_n\varphi^{2n}\beta^{-2n}\right), \tag{27}$$

where

$$A_n\equiv 2(-1)^n(2^{2n-1}-1)\left(\frac{\pi}{A}\right)^{2n}\frac{B_n}{(2n)!} \tag{28}$$

and B_n are Bernoulli numbers $(B_1=1/6,B_2=1/30,\ldots)$ to obtain

$$I_{\pm}(\beta)=4\pi\beta^{-1}\left(c_{\pm}+\sum_{n=1}^{\infty}\gamma_n^{\pm}\beta^{-2n}\right), \tag{29}$$

where $c_+\equiv A/q_0$, $c_-\equiv q_1/q_0$,

$$\gamma_n^+\equiv\frac{A_n}{A}\int_0^{\infty}\varphi^{2n}e^{-\varphi}\cos(p\varphi)d\varphi,$$

$$\gamma_n^-\equiv\frac{A_n}{A}\int_0^{\infty}\varphi^{2n}e^{-\varphi}\sin(p\varphi)d\varphi, \tag{30}$$

and we made use of expressions $\int_0^{\infty}e^{-\varphi}\cos(p\varphi)d\varphi=(1+p^2)^{-1}$ and $\int_0^{\infty}e^{-\varphi}\sin(p\varphi)d\varphi=p(1+p^2)^{-1}$. Making use of Eq. (29) into Eq. (23), taking into account the expressions $\int_0^{\infty}\varphi^2e^{-\varphi}\cos(p\varphi)d\varphi=-2(3p^2-1)(1+p^2)^{-3}$ and

$\int_0^\infty \varphi^2 e^{-\varphi} \sin(p\varphi)d\varphi = -2p(p^2-3)(1+p^2)^{-3}$, we get

$$H_0(\beta) = \frac{4}{q_0} + \frac{4}{A}\sum_{n=1}^{\infty} \gamma_n^+ \beta^{-2n},$$

$$H_1(\beta) = 4\beta\sum_{n=1}^{\infty} (p\gamma_n^+ - \gamma_n^-)\beta^{-2n}. \tag{31}$$

By plugging Eq. (31) into Eq. (16) and making use of the expressions $\int_0^\infty \varphi^4 e^{-\varphi} \cos(p\varphi)d\varphi = 24(1-10p^2+5p^4)(1+p^2)^{-5}$ and $\int_0^\infty \varphi^4 e^{-\varphi} \sin(p\varphi)d\varphi = 24p(5-10p^2+p^4)(1+p^2)^{-5}$, one finally obtains the kinetic coefficients in the polynomial form

$$J_0 = Bc_0\left(J_{00} + J_{02}\beta^{-2} + \sum_{n=2}^{\infty} J_{0,2n}\beta^{-2n}\right),$$

$$J_1 = Bc_0\left(J_{11}\beta^{-1} + \sum_{n=2}^{\infty} J_{1,2n-1}\beta^{-2n+1}\right),$$

$$J_2 = Bc_0\left(J_{20} + J_{22}\beta^{-2} + \sum_{n=3}^{\infty} J_{2,2(n-1)}\beta^{2(1-n)}\right), \tag{32}$$

where

$$J_{00} \equiv \frac{3n_0}{\pi^2 q_0}, \quad J_{20} \equiv \frac{n_0}{q_0}, \quad J_{02} \equiv 1 + \frac{q_2}{q_0^3},$$

$$J_{11} \equiv a_1 + \frac{q_3}{q_0^2}, \quad J_{22} \equiv \frac{7\pi^2}{5}\left(1 + \frac{q_4}{q_0^4}\right),$$

$$J_{0,2n} \equiv \frac{3}{\pi^2}(A^{-1}a_7\gamma_n^+ - a_3\gamma_n^-),$$

$$J_{1,2n-1} \equiv \frac{3}{\pi^2}(A^{-1}a_8\gamma_n^+ - a_5\gamma_n^-),$$

$$J_{2,2(n-1)} \equiv \frac{3}{\pi^2}(A^{-1}a_9\gamma_n^+ - a_6\gamma_n^-), \tag{33}$$

and $q_2 \equiv 2a_3q_0q_1 + a_4(4q_1^2 - q_0)$, $q_3 \equiv 2a_5q_1 - a_3(4q_1^2 - q_0)$, $q_4 \equiv q_0q_2$, $a_7 \equiv a_4 + a_3q_1$, $a_8 \equiv a_5q_1 - a_3q_0$, and $a_9 \equiv a_6q_1 - a_5q_0$.

In the low-temperature limit ($\beta^{-1} \to 0$) the kinetic coefficients reduce to the zeroth order terms in Eq. (32) so that the corresponding transport coefficients read

$$\sigma(T) \to \sigma_0, \quad S(T) \simeq -\frac{k_B^2 J_{11}}{|e|J_{00}}T, \quad \kappa_e(T) \simeq \sigma_0 L_0 T,$$

where $\sigma_0 \equiv c_0 n_0 q_0^{-1}$ measures the residual conductivity of the sample. As we can see, both thermopower and thermal conductivity go linearly to zero when the temperature is progressively decreased, whereas the electrical conductivity reaches its residual value at $T=0$, as expected. The linear dependence of thermopower in the low-temperature limit indicates that one can confidently use Mott's formula in the analysis of Seebeck coefficient for CMAs in this case. Analogously, the WFL is also obeyed in the low-temperature regime and the Lorenz number is given by Sommersfeld's value L_0.

Transport coefficients corresponding to the intermediate temperature regime can be obtained from Eq. (32) by considering additional terms in the kinetic coefficient polynomials. In order to compare with thermal-conductivity experimental curves, it will suffice with the following expressions as a first approximation:

$$\kappa_e(T) = \frac{1 + QT^2 + RT^4}{1 + \frac{J_{02}}{J_{00}}k_B^2T^2 + \frac{J_{04}}{J_{00}}k_B^4T^4}\sigma_0 L_0 T, \tag{34}$$

$$L(T) = \frac{1 + QT^2 + RT^4}{1 + 2\frac{J_{02}}{J_{00}}k_B^2T^2 + \left[\left(\frac{J_{02}}{J_{00}}\right)^2 + 2\frac{J_{04}}{J_{00}}\right]k_B^4T^4}L_0, \tag{35}$$

where

$$Q \equiv \frac{J_{02}J_{20} + J_{00}J_{22} - J_{11}^2}{J_{00}J_{20}}k_B^2,$$

$$R \equiv \frac{J_{24}J_{00} + J_{22}J_{02} + J_{04}J_{20} - 2J_{11}J_{13}}{J_{00}J_{20}}k_B^4. \tag{36}$$

III. DISCUSSION

Taking into account Eq. (17) in Eq. (33) we get the nested relationships

$$J_{11} = \frac{2}{q_0^2}(n_0q_1 - n_1q_0),$$

$$J_{02} = \frac{1}{q_0}\left(n_2 - \frac{\pi^2}{3}J_{00} + 2q_1J_{11}\right),$$

$$J_{22} = \frac{7\pi^2}{5}J_{02},$$

$$J_{13} = -\frac{14\pi^2}{5q_0^2}\left(n_3q_0 - n_2q_1 + \frac{q_0 - 4q_1^2}{2}J_{11} + \frac{\pi^2}{3}q_1J_{00}\right),$$

$$J_{04} = \frac{2q_1}{q_0}J_{13} + \frac{7\pi^2}{5q_0^2}(q_0 + J_{20} - 2q_1J_{11} - n_2),$$

$$J_{24} = \frac{155\pi^2}{49}J_{04}, \tag{37}$$

so that making use of the electronic model parameters listed in Table V we can evaluate the values of the kinetic coefficients J_{ij} appearing in Eqs. (34) and (35). In this way, the temperature dependence of both the electronic contribution to the thermal conductivity and the Lorenz function can be explicitly determined. In Fig. 2 we show the temperature dependence of the normalized Lorenz function for the four considered samples. In the limit of very low temperatures

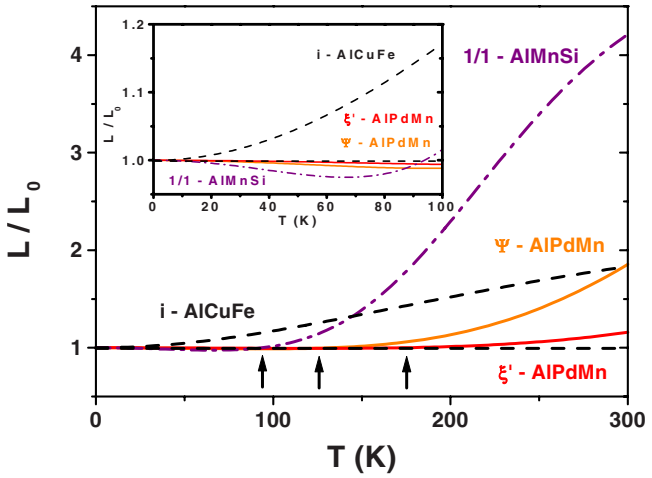

FIG. 2. (Color online) Temperature variation in the normalized Lorenz function corresponding to the samples listed in Table V. The anomalous transport onset temperatures T_o are indicated by vertical arrows in the main frame (more details in the text).

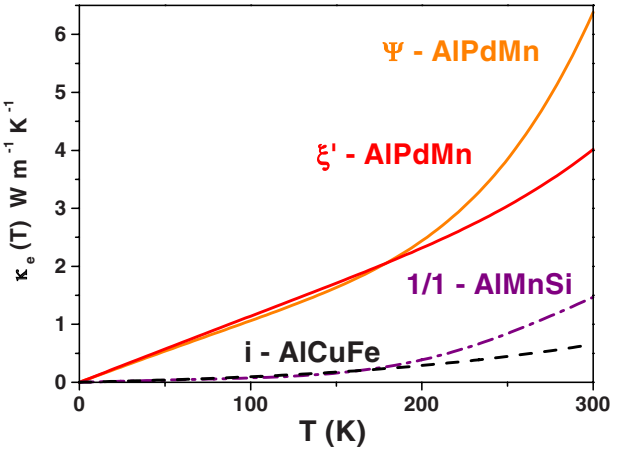

FIG. 3. (Color online) Temperature variation in the electronic contribution to the thermal conductivity for the samples listed in Table V.

(see the inset) the WFL is satisfied, as expected, but as the temperature is progressively increased the Lorenz function deviates from the ideal behavior $L(T)/L_0=1$ (indicated by a dashed horizontal line). The character of this deviation is given by a systematic significant increase in the $L(T)/L_0$ ratio in the case of the quasicrystal whereas this ratio moderately decreases (as usually observed in most alloys[41]) for the remaining samples. The magnitude of the WFL deviation at low temperatures is more pronounced for the approximant phase than for the giant unit-cell phases. As the temperature is progressively increased the character of the WFL deviation progressively turns from $L(T)/L_0<1$ to $L(T)/L_0>1$ at the temperature values $T_o \simeq 90$ K, $T_o \simeq 130$ K, and $T_o \simeq 170$ K for the 1/1-AlMnSi, Ψ-AlPdM, and ξ'-AlPdMn phases, respectively (mainframe arrows). Thus, the temperature interval over which the WFL is satisfied strongly depends on the considered sample, and it is considerably wider for the giant unit cell ξ' and Ψ-AlPdMn phases than for the approximant and quasicrystalline phases, respectively. This trend agrees with the typically metallic behavior of the former samples, which is characterized by positive temperature coefficients of the electrical resistivity and negative small values of the thermopower in the considered temperature range.[34] By comparing the $L(T)/L_0$ curves shown in Fig. 2 with the transport coefficient temperature dependence of the 1/1-AlMnSi sample we also realize that the relatively sudden growth of the $L(T)/L_0$ curve, starting at about 100 K, nicely correlates with a change in the electrical conductivity slope from negative to positive temperature dependence, as well as the presence of a shallow minimum in the $S(T)$ curve at about 150 K.[33] The existence of a characteristic temperature indicating the onset of an anomalous behavior in the Lorenz function for each considered sample confirms the existence of different temperature scales in CMAs, presumably related to the presence of different scale lengths in their spatial structure. In fact, the sequence of appearance of the turning points in the $L(T)/L_0$ curves is directly correlated with the corresponding unit-cell density, hence disclosing a relationship between the anomalous transport properties, onset temperature T_o and a characteristic size measured in terms of the unit-cell density (N/V) (Table VI). Note, however, that quasicrystals occupy an odd position within this tentative classification scheme since they exhibit an anomalous behavior starting at the lowest possible temperature.

In Fig. 3 we show the temperature dependence of the electronic contribution to the thermal conductivity for the considered samples obtained from Eq. (34). Quasicrystalline and approximant phases exhibit remarkably low-$\kappa_e(T)$ values (below 1 W m^{-1} K^{-1}) over the entire temperature range, whereas giant unit-cell samples exhibit a significantly steeper

TABLE VI. The anomalous transport property onset temperature T_o (see Fig. 2) is listed along with the main structural parameters for the CMAs considered in this work. Quasicrystals are considered as having an infinite size effective unit cell. The approximant phase has a cubic unit cell composed of MacKay clusters. ξ' and Ψ phases have an orthorhombic unit cell composed of MacKay clusters. N is the number of atoms in the unit cell.

Sample	T_0 (K)	a (nm)	b (nm)	c (nm)	V (nm^3)	N	Ref.
$1/1Al_{73.6}Mn_{17.4}Si_9$	90	1.260			2.000	138	5
ξ'-$Al_{73}Pd_{22.9}Mn_{4.1}$	170	2.354	1.656	1.234	4.810	320	23
Ψ-$Al_{72.9}Pd_{22.9}Mn_{4.2}$	130	2.354	1.656	5.700	22.220	1500	23
i-$Al_{63}Cu_{25}Fe_{12}$	0				∞	∞	

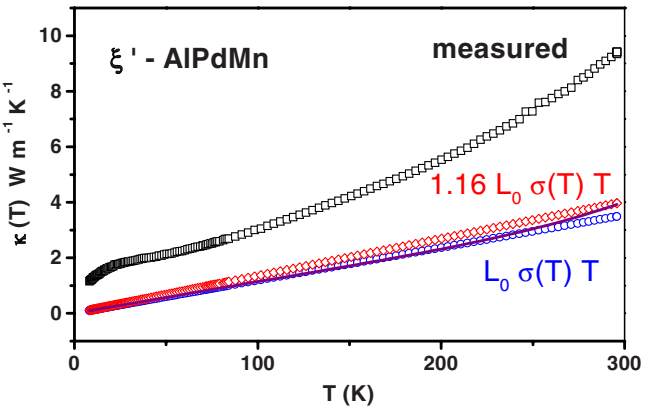

FIG. 4. (Color online) The temperature dependence of the measured thermal conductivity (squares) is plotted along with the electronic contribution derived from Eq. (34) (solid line), Eq. (3) (diamonds), and the standard WFL expression $\kappa_e(T)=L_0T\sigma(T)$ (circles). Experimental data by courtesy of Dolinšek.

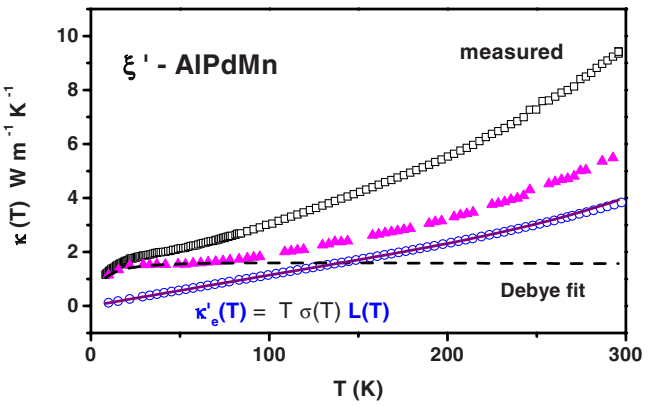

FIG. 5. (Color online) The lattice contribution to the thermal conductivity (triangles) is derived by subtracting to the experimentally measured thermal conductivity (squares) the charge-carrier contribution making use of Eq. (34) (solid line) and Eq. (35) (circles). Experimental data by courtesy of Dolinšek (for more details see the text).

slope leading to $\kappa_e(T)$ values about 1 order of magnitude larger in the temperature range of 100–300 K. In order to check the feasibility of these theoretically derived $\kappa_e(T)$ curves, in Fig. 4 we compare that corresponding to the ξ'-AlPdMn sample (which according to Fig. 2 obeys the WFL over a wider temperature interval) with suitable experimental data. As we can see the agreement between the analytical curve obtained from Eq. (34) and those derived from the experimentally measured electrical conductivity is excellent. This result opens up the possibility of using our phenomenological approach in order to derive the electronic contribution to the thermal conductivity in an alternative way, which does not rely on the validity of the WFL. The basic steps of such a procedure are the following ones: (1) the experimental $\sigma(T)$ and $S(T)$ curves are fitted to the expressions[32–34]

$$\sigma(T) = \sigma_0(1 + c_2T^2 + c_4T^4 + c_6T^6),$$

$$S(T) = -0.0488T\frac{a + fT^2 + gT^4}{1 + c_2T^2 + c_4T^4 + c_6T^6}, \qquad (38)$$

where the electrical conductivity is expressed in $(\Omega\,\mathrm{cm})^{-1}$ and the Seebeck coefficient is expressed in $\mu\mathrm{V\,K}^{-1}$. The fitting parameters are related to a series of coefficients ξ_n (which can be regarded as phenomenological parameters containing information about the electronic structure of the sample) through the relationships $\xi_1 \equiv a$, $\xi_2 \equiv c_2/b$, $\xi_3 \equiv f/b$, and $\xi_4 \equiv c_4/b^2$. (2) Following the algebraic procedure described in the appendix of Ref. 33, we get the electronic model parameters $\{\alpha, \gamma_i, \delta_i\}$ determining the spectral-conductivity function given by Eq. (5) making use of the phenomenological coefficients ξ_n. (3) Finally, from the knowledge of the above electronic model parameters we determine the kinetic coefficients J_{ij} after Eq. (37) and then derive the analytical expression for $\kappa_e(T)$ from Eq. (34).

In this way, though we do not make explicit use of the WFL, we still determine the electronic contribution to the thermal conductivity from experimental data related to the transport properties of the considered sample. In particular, the fitting analysis prescribed in step 1 properly *combines* experimental data related to the transport coefficients $\sigma(T)$ and $S(T)$. In so doing, one discloses relevant information about the electronic structure of the sample enclosed in the temperature dependence of these transport coefficients.

The convenience of such an approach for a proper analysis of the lattice contribution to the thermal conductivity is illustrated in Fig. 5, where the $\kappa_e(T)$ contribution derived from Eq. (34) (solid line) is compared with that obtained from the expression $\kappa_e'(T)=T\sigma_{\mathrm{exp}}(T)L_{\mathrm{th}}(T)$ (circles), where $\sigma_{\mathrm{exp}}(T)$ are experimental data[42] and $L_{\mathrm{th}}(T)$ has been derived from Eq. (35). The excellent agreement between both curves confirms the consistency of the adopted approach. Then, we determine the lattice contribution to the thermal conductivity as $\kappa_{\mathrm{ph}}(T)=k_m(T)-\kappa_e'(T)$ (triangles), where $k_m(T)$ is the measured thermal conductivity including contributions from both charge carriers and phonons (squares). As we can see, the anomalous enhancement of the WFL at relatively high temperatures (see Fig. 2) cannot completely explain the anomalous increase in the thermal conductivity measured in this sample (squares). In fact, by comparing the resulting $\kappa_l(T)$ curve with a fit to Eq. (4), as reported in Ref. 23 (dashed line), we appreciate that some additional contribution coming from the lattice itself should be invoked in the temperature range of 100–300 K.

IV. CONCLUSIONS

Spurred by a series of experimental facts, indicating significant enhancements of the Lorenz number with respect to standard Sommerfeld's value, in this work we have revisited the applicability of the WFL given by the expression $\kappa_e(T)=L_0T\sigma(T)$ in CMAs. To this end, we have obtained closed analytical expressions for the $\kappa_e(T)$ and $L(T)$ transport coefficients. In the limit of very low temperatures the WFL is satisfied, as expected, but as the temperature is progressively increased the Lorenz function deviates from the ideal behav-

ior $L(T)/L_0=1$. Whereas the quasicrystalline sample exhibits a systematic and significant deviation for all the considered temperatures, the other samples show the existence of a characteristic temperature signaling the onset of the anomalous behavior. This characteristic temperature is directly related to the unit-cell density of the sample and progressively takes on larger values as this density decreases. The absence of such a temperature in the quasicrystalline sample is interpreted on the basis of the existence of an effective unit cell of infinite effective size in this alloy class. Since a direct application of the WFL seems to be inappropriate in most CMAs at both intermediate and high-temperature ranges, we propose an alternative route to derive the lattice contribution to the thermal conductivity based on a simultaneous fitting analysis of the electrical conductivity $\sigma(T)$ and thermoelectric power $S(T)$ experimental transport curves in a systematic way. As an illustrative example we have derived the lattice contribution to the thermal conductivity for a ξ'-AlPdMn sample. According to the obtained results the systematic increase in the thermal conductivity reported for this material cannot be completely explained in terms of the Lorenz function enhancement given by Eq. (35) and some additional physical mechanism must be at work. In order to further clarify the precise physical nature of such a processes additional studies of thermal-transport properties in different CMAs would be pertinent.

ACKNOWLEDGMENTS

I am indebted to Jean Marie Dubois for his kind invitation to participate in the workshop *Frontiers in Complex Metallic Alloys* recently held in Zagreb, as a part of the activities of the Sixth Framework European Network of Excellence "Complex Metallic Alloys." I warmly thank Ana Smontara for her kind hospitality when visiting the Institute of Physics in Zagreb and Ivo Batistić, Ante Bilušić, and Denis Stanić for interesting conversations. I am also indebted to Tsunehiro Takeuchi for insightful thoughts, to Janez Dolinšek for sharing with me his experimental data, and to Rogelio Rodríguez-Oliveros for his useful collaboration. I thank M. Victoria Hernández for a critical reading of the paper. This work has been supported by the Universidad Complutense de Madrid and Banco Santander under Project No. PR34/07-15824.

*emaciaba@fis.ucm.es

[1] J. M. Dubois, in *Basics of Thermodynamics and Phase Transitions in Complex Metallic Alloys*, Book Series on Complex Metallic Alloys Vol. 1, edited by Esther Belin-Ferré (World Scientific, Singapore, 2008), pp. 2–6; M. G. Barthès-Labrousse and J. M. Dubois, Philos. Mag. **88**, 2217 (2008).
[2] E. Belin-Ferré, M. Klanjšek, Z. Jagličić, J. Dolinšek, and J. M. Dubois, J. Phys.: Condens. Matter **17**, 6911 (2005).
[3] J. M. Dubois, *Useful Quasicrystals* (World Scientific, Singapore, 2005), p. 137.
[4] J. M. Dubois, J. Phys.: Condens. Matter **13**, 7753 (2001).
[5] T. Takeuchi, N. Nagasako, R. Asahi, and U. Mizutani, Phys. Rev. B **74**, 054206 (2006).
[6] K. Giannò, A. V. Sologubenko, M. A. Chernikov, H. R. Ott, I. R. Fisher, and P. C. Canfield, Phys. Rev. B **62**, 292 (2000).
[7] A. Smontara, I. Smiljanić, A. Bilušić, Z. Jagličić, M. Klanjšek, S. Roitsch, J. Dolinšek, and M. Feuerbacher, J. Alloys Compd. **430**, 29 (2007).
[8] A. M. Strydom, J. Phys.: Condens. Matter **19**, 386205 (2007).
[9] Y. K. Kuo, K. M. Sivakumar, H. H. Lai, C. N. Ku, S. T. Lin, and A. B. Kaiser, Phys. Rev. B **72**, 054202 (2005).
[10] Y. Muro, T. Sasakawa, T. Suemitsu, T. Takabatake, R. Tamura, and S. Takeuchi, Jpn. J. Appl. Phys., Part 1 **41**, 3787 (2002).
[11] S. Paschen, W. Carrillo-Cabrera, A. Bentien, V. H. Tran, M. Baenitz, Y. Grin, and F. Steglich, Phys. Rev. B **64**, 214404 (2001).
[12] A. Bilušić, Ž. Budrović, A. Smontara, J. Dolinšek, P. C. Canfield, and I. R. Fisher, J. Alloys Compd. **342**, 413 (2002).
[13] Y. K. Kuo, J. R. Lai, C. H. Huang, C. S. Lue, and S. T. Lin, J. Phys.: Condens. Matter **15**, 7555 (2003).
[14] T. Takeuchi, T. Otagiri, H. Sakagami, T. Kondo, U. Mizutani, and H. Sato, Phys. Rev. B **70**, 144202 (2004).
[15] N. W. Ashcroft and N. D. Mermin, *Solid State Physics* (Saunders, Cornell, 1976), p. 255.
[16] Yu. K. Vekilov, E. I. Isaev, and B. Johansson, Phys. Lett. A **352**, 524 (2006).
[17] D. Mayou, in *Quasicrystals Current Topics*, edited by E. Belin-Ferré, C. Berger, M. Quiquandon, and A. Sadoc (World Scientific, London, 2000), pp. 445–447.
[18] E. Maciá, Appl. Phys. Lett. **81**, 88 (2002).
[19] C. V. Landauro, E. Maciá, and H. Solbrig, Phys. Rev. B **67**, 184206 (2003).
[20] E. Maciá and R. Rodríguez-Oliveros, Phys. Rev. B **75**, 104210 (2007).
[21] A. Perrot and J. M. Dubois, Ann. Chim. (Fr.) **18**, 501 (1993).
[22] Z. Bihar, A. Bilušić, J. Lukatela, A. Smontara, P. Leglić, P. J. McGuiness, J. Dolinšek, Z. Jagličić, J. Jamovec, V. Demange, and J. M. Dubois, J. Alloys Compd. **407**, 65 (2006).
[23] J. Dolinsek, P. Jeglic, P. J. McGuiness, Z. Jaglicic, A. Bilusic, Z. Bihar, A. Smontara, C. V. Landauro, M. Feuerbacher, B. Grushko, and K. Urban, Phys. Rev. B **72**, 064208 (2005).
[24] J. Dolinšek, S. Vrtnik, M. Klanjšek, Z. Jagličić, A. Smontara, I. Smiljanić, A. Bilušić, Y. Yokoyama, A. Inoue, and C. V. Landauro, Phys. Rev. B **76**, 054201 (2007).
[25] P. A. Kalugin, M. A. Chernikov, A. Bianchi, and H. R. Ott, Phys. Rev. B **53**, 14145 (1996).
[26] A. Bilušić, A. Smontara, J. Dolinšek, P. J. McGuiness, and H. R. Ott, J. Alloys Compd. **432**, 1 (2007).
[27] A. Smontara, I. Smiljanić, A. Bilušić, B. Grushko, S. Balanetsky, Z. Jagličić, S. Vrtnik, and J. Dolinšek, J. Alloys Compd. **450**, 92 (2008).
[28] C. Janot, Phys. Rev. B **53**, 181 (1996).
[29] C. V. Landauro and H. Solbrig, Mater. Sci. Eng., A **294-296**, 600 (2000); Physica B **301**, 267 (2001).
[30] U. Mizutani, T. Takeuchi, and H. Sato, Prog. Mater. Sci. **49**, 227 (2004).

[31] G. Trambly de Laissardière, D. Nguyen-Manh, and D. Mayou, Prog. Mater. Sci. **50**, 679 (2005).
[32] E. Maciá, *Aperiodic Structures in Condensed Matter: Fundamentals and Applications* (CRC, Boca Raton, 2009), pp. 98–124.
[33] E. Maciá, T. Takeuchi, and T. Otagiri, Phys. Rev. B **72**, 174208 (2005).
[34] E. Maciá and J. Dolinšek, J. Phys.: Condens. Matter **19**, 176212 (2007).
[35] E. Maciá, Phys. Rev. B **69**, 132201 (2004).
[36] Temperature-dependent Fermi-level effects in the transport properties were discussed in Ref. 35.
[37] Note the presence of the absolute value of frequency in the integrand, which was inadvertently omitted in Ref. 20.
[38] R. Rodríguez-Oliveros, Master thesis, Universidad Complutense de Madrid, Madrid, 2007.
[39] T. M. Apostol, *Introduction to Analytic Number Theory* (Springer-Verlag, New York, 1995).
[40] O. Espinosa and V. H. Moll, Ramanujan J. **6**, 449 (2002).
[41] U. Mizutani, *Introduction to the Electron Theory of Metals* (Cambridge University Press, Cambridge, 2001), pp. 299–302.
[42] J. Dolinšek, Z. Jagličić, and A. Smontara, Philos. Mag. **86**, 671 (2006).